Cement and Concrete Research 42 (2012) 1014–1023

Contents lists available at SciVerse ScienceDirect

Cement and Concrete Research

journal homepage: http://ees.elsevier.com/CEMCON/default.asp

Study of cracking due to drying in coating mortars by digital image correlation

T. Mauroux [a,b,c], F. Benboudjema [b,*], P. Turcry [a], A. Aït-Mokhtar [a], O. Deves [c]

[a] University of La Rochelle, LaSIE — CNRS FRE 3474, France
[b] ENS Cachan, LMT — CNRS UMR8535, UPMC, PRES-UniverSud Paris, France
[c] CSTB Marne-la-Vallée, France

ARTICLE INFO

Article history:
Received 9 February 2011
Accepted 3 April 2012

Keywords:
Crack detection (B)
Image analysis (B)
Drying (A)
Shrinkage (C)
Coating mortar

ABSTRACT

Drying shrinkage of coating mortars may induce cracks which could result in debonding and reduce the durability of the 'mortar/substrate' system. In order to study this phenomenon, a new device based on digital image correlation (DIC) was developed so as to measure 2D displacement fields on mortars and substrates at early age in drying conditions. Compared to intrusive methods (e.g. SEM observation, embedded rigid sensor) or impregnation techniques, the proposed device does not induce parasite cracks and specimen can be monitored continuously and automatically. Moreover, representative geometries and restraint conditions can be tested. A post-processing tool is proposed to determine the evolution of the cracking patterns by computing an equivalent strain. Besides, this enables the quantification of the widths and the depths of cracks inside the mortar and at the mortar/substrate interface. The device was validated by comparison with measurements of drying shrinkage using LVDT and investigations with an optical microscope. It was used successfully to analyze drying shrinkage cracking of coating mortars due to restraint by a rigid substrate.

1. Introduction

The durability of coating mortars is strongly affected by cracking due to drying shrinkage and the quality of the adhesion with the substrate [1–6]. Due to cracking, diffusivity and permeability of the material may increase by several orders of magnitude [7,8]. Therefore, the main challenge is to avoid or control cracking which can create debonding, as shown in Fig. 1 [6].

The main modes of failure in mortar/substrate systems are tensile cracking through the mortar thickness and peeling or shearing at the interface between both materials [3–5,9–11]. The main sources of cracking are stresses induced by restrained drying shrinkage. The development at the early age of this stress state is very complex. It is strongly heterogeneous in the mortar thickness (Fig. 1) due to the combination of several phenomena, such as hydration, drying, evolution of mechanical properties, and creep.

Many tests were proposed in literature to analyze the behavior of mortar/substrate systems at early age. One example is the ring-test, which consists in casting a mortar ring around a metallic ring (modeling the substrate rigidity) for the determination of stresses in mortar or concrete [12–15]. However, the metallic surface is not physically and chemically representative of real substrates, such as concrete or bricks. Besides, the stiffness of the metallic ring is different from the one of a real substrate. Thus, a modeling tool is required to analyze accurately the experimental results [15]. Despite these shortcomings, the ring-test remains the most widely used test for studying the drying shrinkage cracking behavior of cement-based materials [16,17].

For concrete repair systems, several authors designed experimental methods with mortar cast on "real" substrates. The determination of the resulting strain in the repair material is conducted thanks to embedded gauges [2,3]. The localization and the pattern direction of gauges are chosen in order to monitor the development of cracks. For monolayer coating mortars, the usual thickness is about 10 mm (limited to 18 mm according to the French Standard NF DTU 26.1 P1-1). This thickness is lower than the usual thicknesses of repair materials (25 to 40 mm) and therefore limits the use of gauges or fiber optic sensors [18,19].

Coating mortars could also be studied thanks to Linear Variable Differential Transformer (LVDT) sensors placed on both sides of a mortar layer [20]. However, this method presents the same problems as methods using embedded gauges: local and oriented measures, no accurate localization of cracks, and possible interactions with stress state evolution in mortar.

Drying shrinkage cracks can also be observed using an optical or a scanning electron microscopy (SEM) e.g. [21–25]. However, for a classical SEM, the preparation of the sample, and especially the placing under vacuum, results in additional (parasite) cracks [21]. Manual observation is only performed at selected locations, providing limited information. The use of impregnation methods helps to identify cracks, but is not easy since the cement paste adjacent to the crack is also impregnated [24]. In addition, this technique does not allow continuous monitoring of the evolution of micro-cracks and drying shrinkage cannot be measured. Some authors have used digital image techniques to monitor displacement fields due to drying shrinkage. For instance,

* Corresponding author.
E-mail address: farid.benboudjema@dgc.ens-cachan.fr (F. Benboudjema).

0008-8846/$ – see front matter © 2012 Elsevier Ltd. All rights reserved.
doi:10.1016/j.cemconres.2012.04.002

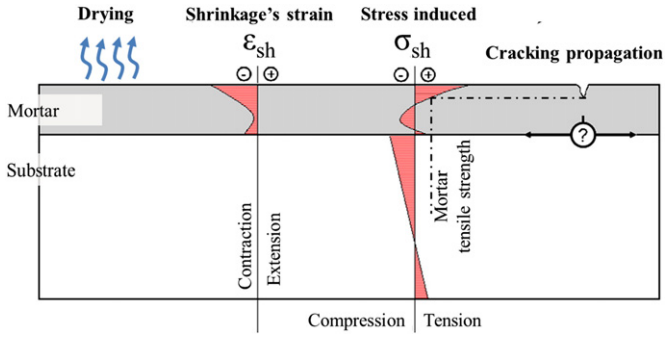

Fig. 1. Development of drying cracks due to self and external restraint in a mortar layer. Adapted from [6].

Neubauer et al. [26] used an image intensity matching technique comparing digital images, but only global data (mapping of drying shrinkage strains) were obtained.

In order to overcome these issues, a new test device to monitor the evolution of shrinkage, the propagation of cracks in mortar and their quantification (location, opening, depth) during drying is proposed in the present paper. It is based on the monitoring of the displacement field by means of digital image correlation (DIC) [27] and a post-processing tool used to capture the mapping of shrinkage strains and cracks at the drying surface or in the (observable) thickness. The same device was used successfully by Lagier et al. [28] in order to study cracking due to restrained shrinkage around aggregates in concrete and cracking in beam (bending) and walls (shearing), tested with quasi-static conditions in the French project called "CEOS" [29].

Our aim is to study the accuracy and the validity of the developed device. For this purpose, two types of test were carried out. In the first type, "free" drying shrinkage was studied with both LVDT sensors and DIC technique. Our objective was to partially validate the DIC technique. In the second type, cracking due to the restraint of drying shrinkage was studied on mortar/substrate systems. Our objective was to show the ability of DIC technique to identify the pattern and the width of cracks (superficial and in-depth). Both cracking of the drying surface and cracking at the interface between mortar and substrate were investigated.

2. Experimental program

2.1. Principles of DIC

Digital image correlation (DIC) is usually used for short term tests on non scalable materials (e.g. metallic or ceramic material). Only few studies have used this method to investigate the behavior of cementitious materials during long periods [25,26,28,30–32]. In the present study, DIC is carried out using Correli-Q4-LMT, a software developed in the LMT laboratory (see http://www.lmt.ens-cachan.fr/PDFs/HILD.2008.7.pdf and [27]) in order to measure displacement fields. Since the principles of this method were previously published by the developers of this software, only the main features are briefly presented below (for more details see aforementioned references).

The digital image correlation method is based on the comparison of two images with two random gray levels recorded before and after a displacement. The first picture is called "reference" and the second "deformed". The correlation consists in determining the degree of similarity (in terms of conservation of optical flux) between these two pictures. The displacement measurement consists in finding the best displacement field which allows overlying the pattern of the "reference" image and those of the "deformed" image using a pattern-matching algorithm. The conservation of the optical flow is a non-linear problem. Kinematic hypotheses are used for the interpolation of displacement fields (QUA4, i.e. 4-node quadrangular finite elements). It leads to a linear system such as systems in finite element problems. To increase the measurable displacement range, a multi-scale setting (sub-pixel interpolation) is used as proposed for a standard DIC algorithm.

One interesting feature of the used software is the possibility to evaluate the a priori performances of the DIC technique through 3 investigations (which were done in the present study):

- The performance of the displacement measurement is largely based on the image texture quality. An analysis of gray level is performed globally not only on the whole surface, but also in each discretized sub-elements.
- Using the original image (f), a translated image (g) is generated by imposing a prescribed translation $\mathbf{u}_{pre}$. The algorithm is then run on the pair of images (f, g) and the estimated displacement field $\mathbf{u}_{est}$ is measured. The quality of the estimation is characterized by two indicators, the systematic error δ_u, and the standard uncertainty σ_u:

$$\delta_u = ||\langle \mathbf{u}_{est}\rangle - \mathbf{u}_{pre}|| \text{ and } \sigma_u = \left\langle ||\mathbf{u}_{est} - \langle \mathbf{u}_{est}\rangle||^2 \right\rangle^{1/2} \quad (1)$$

  where $\langle . \rangle$ and $||.||$ represent the mean and the quadratic norm operators, respectively.
- The effect of noise on the displacement measurement due to the image acquisition (e.g. digitization, read-out noise, black current noise, photon noise), the lighting (see Section 2.3.1) or the CCD sensor, is evaluated. The reference image (f) is corrupted by a Gaussian noise of zero mean. No displacement field is superimposed on the image, and the displacement field is then estimated (g). This analysis allows to estimate the displacement resolution.

2.2. Materials

The mix-proportions of the studied mortar are given in Table 1. The high value of the water to cement ratio (w/c = 1) was imposed by the industrial consortium CEReM who supported this research program (see [33] for instance). The mortar contains a hydroxyl-methyl-propyl cellulose (HMPC) addition. This chemical admixture, which has water retention properties, is currently used in industrial mortars to modify their rheological and mechanical properties [34]. Its impact on microstructure and adherence of mortars is still not well mastered (the study of the influence of ether cellulose content on the mortar properties is ongoing and is beyond the scope of the present paper).

Standardized concrete blocks with cubic dimensions ($20 \times 20 \times 20\ cm^3$) were used as substrate for the restrained shrinkage test described in Section 2.3.2. These commercially available blocks (provided by Rocholl GMBH company) comply with the European Standard EN 1766:2000 on concrete substrates designed for repair materials testing. Since the roughness of the substrate is a major parameter involved in adherence and cracking [35,36], its control is crucial to obtain reproducible test. The surfaces of the blocks were sandblasted with a blasting depth of 1–2 mm.

2.3. Experimental procedures

2.3.1. Free drying shrinkage tests

2.3.1.1. Ambient conditions. Drying shrinkage was measured by LVDT and DIC in the same conditions. Tested specimens were protected

Table 1
Composition of the studied mortar.

Siliceous sand	Portland cement (CEM I 52.5 type)	Siliceous filler (Sifraco)	Cellulosic ether (MHPC)	W/C
650 kg/m^3	300 kg/m^3	50 kg/m^3	0.11%[a]	1

[a] % by weight of the cement content.

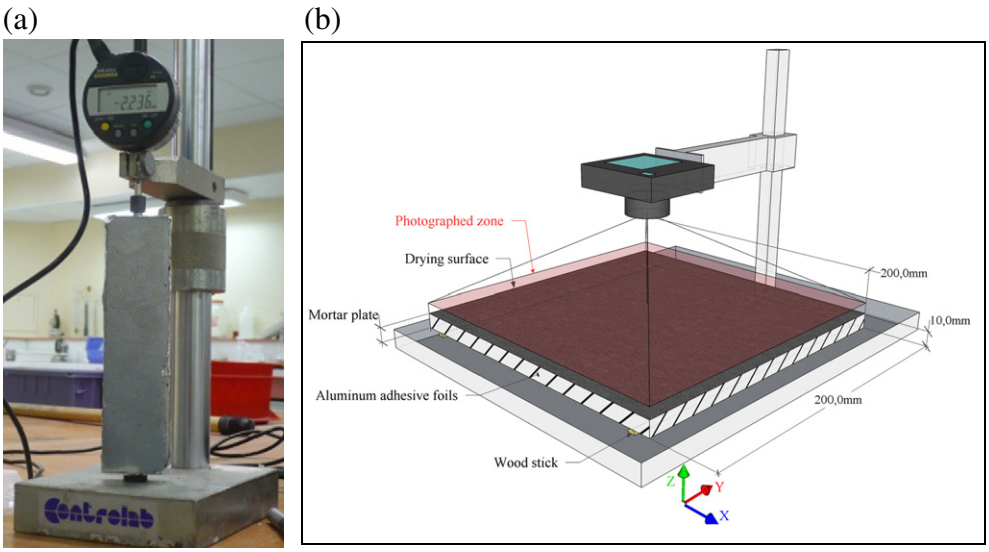

Fig. 2. Experimental devices for measurements of free drying shrinkage: a) LVDT comparator, b) DIC procedure.

from drying by a cellophane film and kept at 25 ± 2 °C for 24 h after mixing. After demolding, they were placed in a room at 25 °C and 30 ± 5% of relative humidity (RH).

2.3.1.2. Measurements with LVDT. The free drying shrinkage of prismatic specimens 2 × 4 × 16 cm was measured by a LVDT sensor (Fig. 2a). Note that autogenous shrinkage was found to be largely negligible for such high w/c ratio [14]. The two opposite lateral faces (2 × 16 cm) and the two end faces (2 × 4 cm) were insulated by adhesive aluminum foils in order to prevent drying by these faces. These hydric boundary conditions were adopted in order to have a symmetrical drying problem and to avoid curling.

2.3.1.3. Measurements based on DIC. Measurements by digital image correlation (DIC) were performed on plates of mortar of 20 × 20 cm² area and 1 cm thickness (Fig. 2b). This geometry corresponds to the one used in the restrained conditions (see Section 2.3.2). The optical device (a CANON EOS 450D camera placed above the mortar surface) was used to monitor the evolution of the upper face displacement. The upper face was the only one in contact with the atmosphere (other sides were protected from drying by adhesive aluminum foils). From the beginning of drying, images (1157 × 1737 pixels) of the surface were recorded every 10 min for 10 days. The time exposure was set to 1 s and the surface was lighted up by several LED lights in order to limit the optical noise. The lower surface was placed

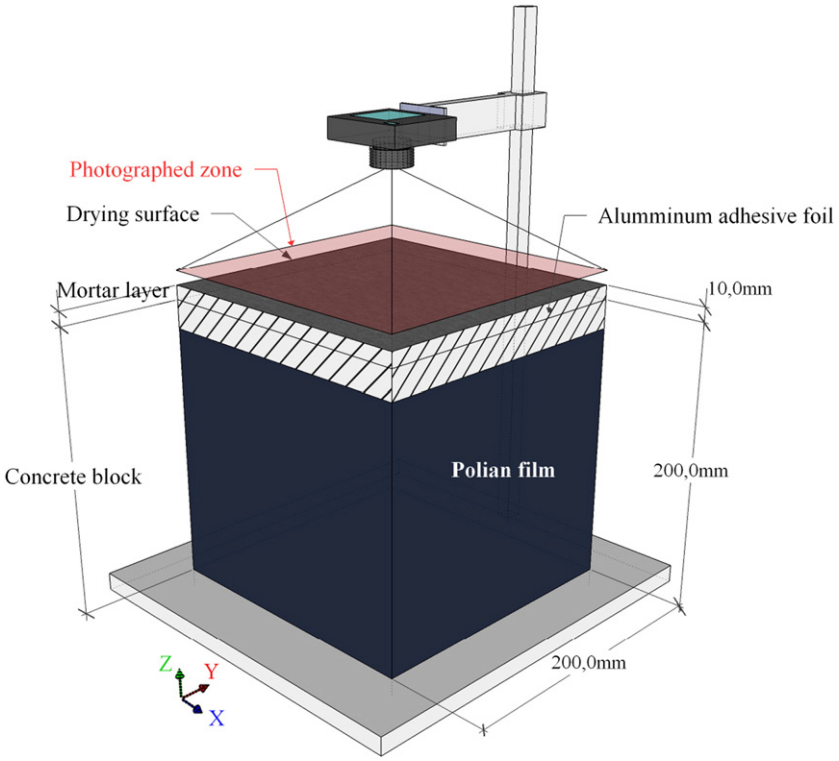

Fig. 3. Restrained shrinkage test: measurement of the surface displacement.

on two wood sticks in order to limit friction (and thus restraint). Therefore, only self-restraint should occur (due to gradients of drying shrinkage between the surface and the core of the specimen [37]). The drying surface of the plate was ink-spotted to obtain a random pattern with a high degree of similarity in order to improve the efficiency of correlation post-processing [27].

2.3.2. Restrained shrinkage tests

Restrained shrinkage tests consisted in measuring by means of DIC the cracking of a mortar cast on a concrete block. During these tests, two kinds of measurement were performed: measurement of the drying surface cracking and measurement of the cracking at the interface between mortar and substrate.

2.3.2.1. Ambient conditions. Concrete blocks were kept for at least 2 weeks in the testing room. Mortar layers of 20 cm² and 1 cm thickness were then cast on these blocks. The mortar was cast vertically thanks to an adapted mold in order to control the layer thickness. After casting, the material was protected from drying for 24 h by the mold and a cellophane film on the upper face. After 24 h, the mold was removed and the upper surface was exposed to drying while the other sides of the specimen were protected by adhesive aluminum foils.

Surface cracking tests were performed under the same conditions to those of free shrinkage tests (i.e. 25 ± 2 °C and R.H. 30 ± 5%). In the case of the cracking interface monitoring, first experiments were performed in the same conditions. For the assessment of the reproducibility, tests were carried out in different conditions in another facility (i.e. 23 ± 2 °C and R.H. 60 ± 5%).

2.3.2.2. Optical device for monitoring surface cracking. The device is similar to the one used for free shrinkage measurement as described in Section 2.3.1 (see Fig. 3).

2.3.2.3. Optical device for monitoring interface cracking. A second device was developed to measure the displacement field at the interface between the mortar and its support. For this purpose, the previous device was used with a glass plate, placed against one lateral side thanks to clamps (as shown in Fig. 4). The other lateral sides were covered by adhesive aluminum foils.

3. Study of free shrinkage by DIC

3.1. Accuracy of DIC algorithm

The performance of DIC computation is linked to the local details of gray level distribution of the image texture [38] (see also Section 2.2). Firstly, a prescribed translation of the original image was performed to obtain a second image. The algorithm was then run on the pair of images in order to estimate the displacement. Comparisons between the imposed and calculated displacement fields were used to evaluate the standard uncertainties and the systematic errors of the algorithm. For large element size, measurement is accurate but estimated over a large zone. On the contrary, for small element size, measurement is spatially resolved but the determination is less accurate [39].

The evaluation of the a priori performance of the DIC technique was undertaken (as explained in Section 2.2). It leads to the choice of a ZOI (zone of interest) size equal to 32 pixels (1 pixel = 0.2 mm). In this case, the associated uncertainty on the displacement was 0.5 μm. This calculation, based on the reference image, gives us only the "intrinsic" accuracy of the algorithm. This uncertainty does not take into account errors due to possible local fluctuations of the measure during the test. The accuracy assessment can be carried out by comparison of measurements from DIC method and measurements from LVDT comparator (Section 3.3).

3.2. Displacement fields

The final displacement fields (after 11 days, along the **x** and **y** directions), calculated by Corelli_Q4_LMT, are given in Fig. 5. Uniform gradients of displacement field along the **x** axis and the **y** axis can be observed. It should be noticed that, in each direction, iso-values of displacement were slightly incurved on the sides of the plate. This phenomenon may be due to a slight drying of the lateral sides induced by the peeling of aluminum adhesive foils. However, no deflection could be observed at the end of the test (the plate was still plane). Thus, no significant displacement out of the measurement plan (due to curling for example) occurred during the test (this was also checked by finite element calculations).

The iso-values reveal a progressive uniform contraction of the plate surface due to drying shrinkage. No gap of displacement can

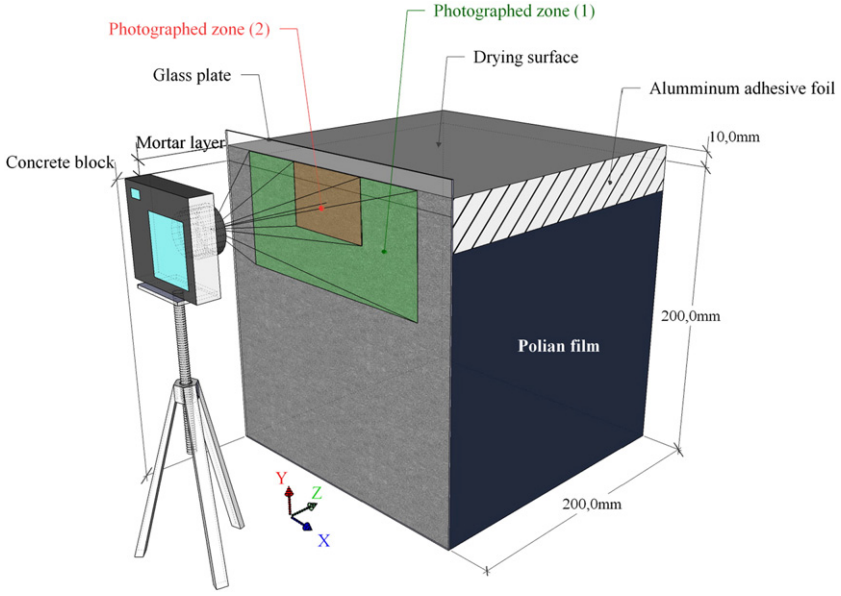

Fig. 4. Restrained shrinkage test: measurements of the displacement field at the interface between the mortar layer and the concrete substrate.

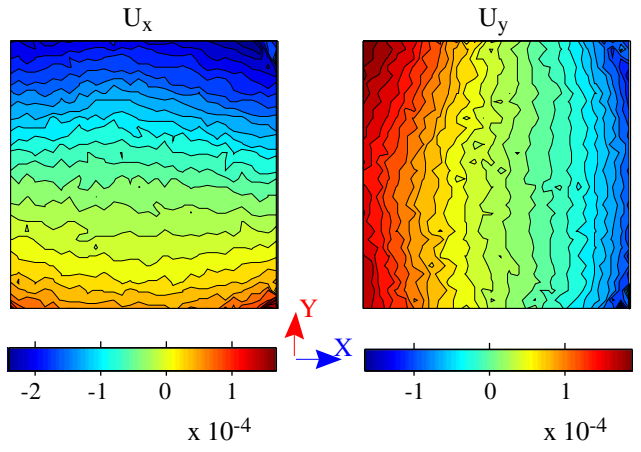

Fig. 5. Field displacements (in m) 11 days after the beginning of the free shrinkage test.

be observed. This means that self-restrain or eventual restrain due to the two wood sticks was not significant. Moreover, except a crack due to formwork removal, no crack or micro-crack was detected (visually or by optical microscopy).

3.3. Comparison between DIC and LVDT measurements

DIC measurements depend strongly on the frame surface quality [38]. In order to validate the proposed procedure, the displacement measured by DIC was used to determine the "mean" strain of the plate. This strain was then compared to the one obtained with a more classical method, i.e. LVDT measurements. In the case of the LVDT comparator, the average strain was obtained by dividing the measured vertical displacement by the specimen length. In the case of DIC, it was achieved by averaging the strain field in each direction (which was obtained by using linear interpolation functions for the displacement fields such as in the case of 4-node finite elements, see Section 2.1 and Eq. (2)).

In order to ensure comparability of the two measurement methods, specimens (prisms and plates) were made from the same batch. Moreover, the drying faces of the prisms used for LVDT measurements were also lighted up with LED lights, so as to obtain the same drying conditions at the mortar surface for both tests.

The evolution and the order of magnitude of strain from the two devices were found close (Fig. 6). The small difference between results may be due to the difference of geometry and the location of measurement points (for the results with LVDT comparator). However, the rather good agreement between the two measurement methods indicates that the DIC method is efficient for obtaining displacement and strain fields during a several days long drying. It should be noted that this efficiency was also verified in literature in the case of drying shrinkage measurements of cement pastes [28] and in the case of mechanical loading strain measurements of others materials, for instance metallic materials or mineral wools [27].

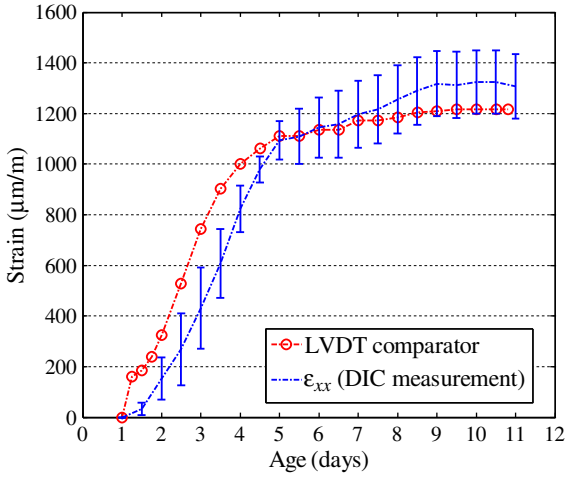

Fig. 6. Free shrinkage strains obtained by DIC procedure and LVDT comparator method.

4. Study of restrained shrinkage by DIC

4.1. Study of surface cracking

4.1.1. Procedure for locating micro-cracks

At the end of the restrained shrinkage test, no macro-crack (i.e. visible to naked eye) was observed. Only micro-cracks (i.e. only visible with optical microscope) on the whole surface were detected. The image correlation reveals also that the displacement field is heterogeneous.

The first step of the post-processing procedure was to conserve displacements higher than the DIC algorithm uncertainty. The determination of the algorithm uncertainty was done as explained in Sections 2.2 and 3.1. It was found equal to 2 µm for the configuration of restrained shrinkage test. Note that a lower value was found for free shrinkage test (i.e. 0.5 µm — see Section 3.1), because the test configurations, such as painting or lightning, were slightly different.

Strain tensor was then calculated thanks to the small strain hypothesis (the displacement gradient is computed after interpolation of the displacement by Q4 finite elements):

$$\boldsymbol{\varepsilon}(\mathbf{x}) = \frac{1}{2}\left(\mathbf{Grad}(\mathbf{U}(\mathbf{x})) + {}^{T}\mathbf{Grad}(\mathbf{U}(\mathbf{x}))\right) \text{ with } \mathbf{U}(\mathbf{x}) = \sum_{i=1}^{i=n} N_i(\mathbf{x})\mathbf{U}_i^e \qquad (2)$$

where ε is the strain tensor (2D) and $\mathbf{U}$ is the displacement vector depending upon the position vector $\mathbf{x}$. N_i are Q4 (linear) scalar shape function (the same function as in finite element calculations), n is the number of nodes and $\mathbf{U^e}$ are the nodal displacements obtained by digital image correction [27,31,39,40].

Cracking due to restraint of shrinkage (cracking in mode I) is related to 1D tension. As conventionally done in continuum damage mechanics for cement-based materials [41], an equivalent tensile (positive) strain $\hat{\varepsilon}$ was computed as follows in order to characterize cracking with a single scalar value:

$$\hat{\varepsilon} = \sqrt{\langle\boldsymbol{\varepsilon}\rangle_+ : \langle\boldsymbol{\varepsilon}\rangle_+} \qquad (3)$$

where $\langle\rangle_+$ is the positive part operator.

From this equivalent strain, the following criterion f can be derived:

$$f = \hat{\varepsilon} - \kappa_0 \qquad (4)$$

where κ_0 is the tensile strain threshold. This allows us to assess accurately damage/cracking in tension knowing the 2D strain tensor.

This criterion, used previously by Lagier et al. [28] for studying drying cracks in cement pastes, is relevant for cement-based materials due to their very low tensile deformability (and low tensile strength).

The post-processing tool (using Matlab©) displays the field of this criterion (only positive values are displayed), which reveals the apparition of a micro-cracking network at the surface (Fig. 7). The pattern of cracks (3 joining cracks) is typical of cracking due to restrained drying shrinkage such as those observed by Laurence [5] on repair mortars or by Colina and Acker [22] on concrete.

After cracking initiation, the global shape of the cracks network remained the same throughout the test. However, the intensity of

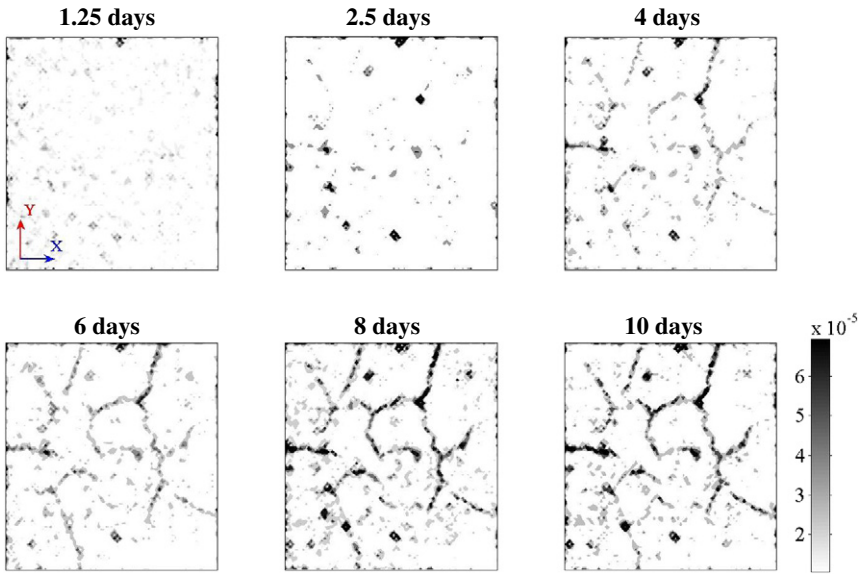

Fig. 7. Micro-cracks pattern on the mortar surface (20×20 cm) during a restrained shrinkage test — Iso-values of equivalent strain of Mazars model in m/m (Time values correspond to successive ages of the tested mortar).

the equivalent tensile strain (Eq. (3)) increased during the test. This suggests an increase of the crack widths. The method does not allow us to determine accurately the time of cracking initiation. Indeed, at this time, the tensile strains are of the same order of magnitude than the resolution of the measure.

4.1.2. Comparison between free shrinkage and damaged area

In order to quantify the evolution of micro-cracks, the ratio of "damaged" elements number on total elements number was calculated. This parameter is relevant because the recorded image includes the entire drying surface. A ZOI is considered "damaged" when its equivalent tensile strain value is higher than 5.10^{-5} m/m. This limit was chosen in agreement with microscopy observation. This calculation was performed without taking into account boundary elements of the image, for which DIC is less accurate (edge effects induced by the assumed periodicity of the signal [40]).

Fig. 8 gives the evolution of this ratio versus the free shrinkage (driving force of cracking) obtained by DIC. Three stages in the development of cracks can be distinguished (as indicated in Fig. 8). It is difficult to interpret the first stage, since there is some noise during this period, as it can be seen for example in Fig. 7 at 1.25 days. During the second stage, the slope of the curve is about 4 times lower than during the third one (after the age of 5 days). Indeed, an increase of 1000 μm of drying shrinkage results in an increase of 2.5% damaged zone content during the second stage, whereas during the third stage a lower increase of shrinkage strain (from 1100 to 1300 μm) results in the same increase of damaged zones content (from 2.5 to 5%). This difference of kinetics may be due to a higher relaxation of stresses due to creep [37,42] and a lower Young modulus of mortar during the second stage than during the third one. Moreover, since cracks appear, they are more and more detectable because of their increase in width, which increases the cracking ratio.

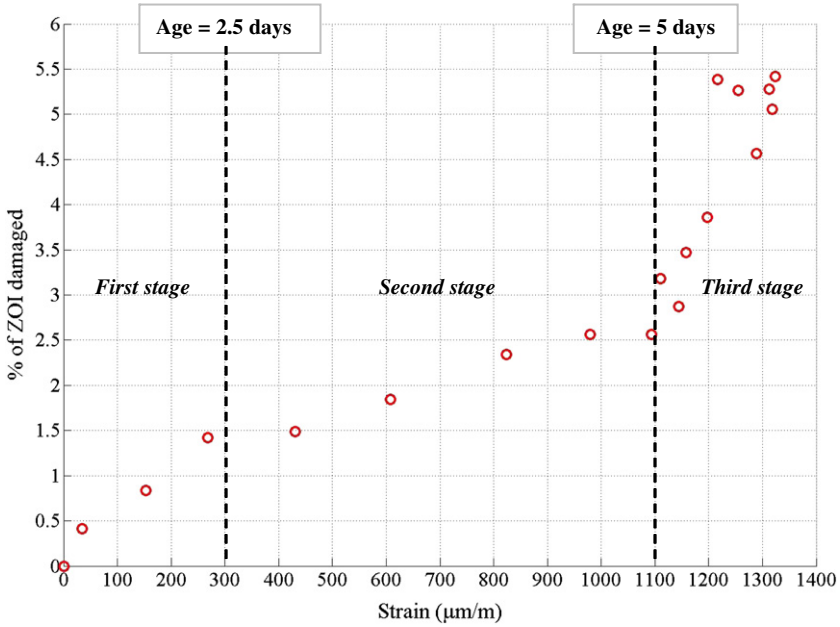

Fig. 8. Damage parameter (defined in Section 4.1.2) deduced from restrained shrinkage test vs. free drying shrinkage obtained by DIC procedure (ages of the tested mortar are also indicated).

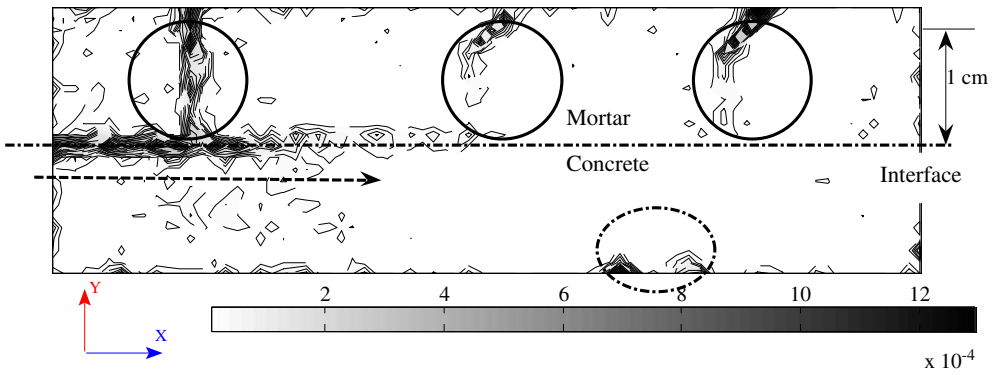

Fig. 9. Map of equivalent tensile strain (in m/m) in the mortar layer and the concrete substrate at the end of the restrained shrinkage test.

4.2. Study of cracking in the mortar and at the mortar/substrate interface

The previously presented method allows us to monitor the global evolution of cracks at the surface. However, it is not enough accurate to determine the time of cracking initiation. Besides, it gives no information on the depth of cracks in the mortar and on the cracking at the interface between mortar and substrate. Thus, a second method was proposed.

4.2.1. Micro-cracking field

First, it should be emphasized that the zone observed by the camera through the glass plate is not representative of the material core (see Fig. 4). However, this zone is subjected to peeling forces which could result in debonding of the mortar layer (Fig. 1). In this experiment, measurements were done on the zone denoted "Zone (1)" in Fig. 4.

Fig. 9 gives the obtained cartography of damaged ZOI. Three micro-cracks (3 circles in straight lines) were detected going from the drying surface to the interface. This failure mode is in agreement with the evolution of the tensile stress during the restrained shrinkage test (see Fig. 1). Moreover, a micro-crack (arrow) at the interface between mortar and substrate was also observed. The shrinkage of the mortar layer induces shear stress, which results in debonding. Each one of these cracks was confirmed by optical microscopy observations.

Note that computations from DIC measurements revealed also a crack (one circle in mixed line) in the concrete substrate. This crack was however not observed by microscopy. This can be considered as an artifact due to the lack of accuracy of DIC algorithm at the border of the "Zone (1)".

4.2.2. Assessment of tensile crack widths

As indicated previously, three tensile cracks propagated through the mortar layer and reached the interface between the two materials. Beyond this qualitative observation, it should be interesting to quantify their crack widths, for example for the determination of their impact on transfer of aggressive agents such as chlorides or CO_2 [43].

Crack widths were determined at the middle of the mortar layer (line A′–B′ in the cartography of damage given in Fig. 10). In order to obtain an accurate measurement, some precautions should be taken. Indeed, the image texture of the ZOI where the crack occurred is modified by the presence of the crack. Consequently, in this zone, it is difficult to associate these "deformed" elements to those of the "reference" image. This results in a loss of accuracy of the image correlation. When crack widths are determined from the difference between displacements at both sides of the crack, the so-obtained widths could be up to 2 times higher than the widths determined by optical microscopy. In order to overcome this issue, displacements were interpolated as shown in Fig. 10. The observed displacement gaps correspond to the cracks. Then, the crack width can be calculated as the difference of displacement between the interpolated displacements at the left and the right sides of crack location. This interpolation method allows us to determine crack widths, for instance 25.6, 16.6 and 14.6 μm in Fig. 10. These values are of the same order of magnitude than those found by microscopy.

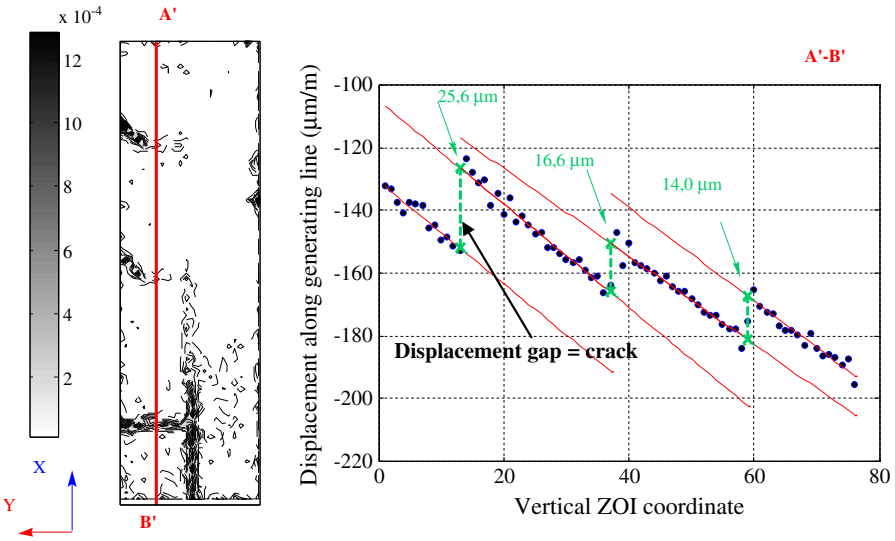

Fig. 10. Determination of tensile crack widths by interpolation from the displacement field.

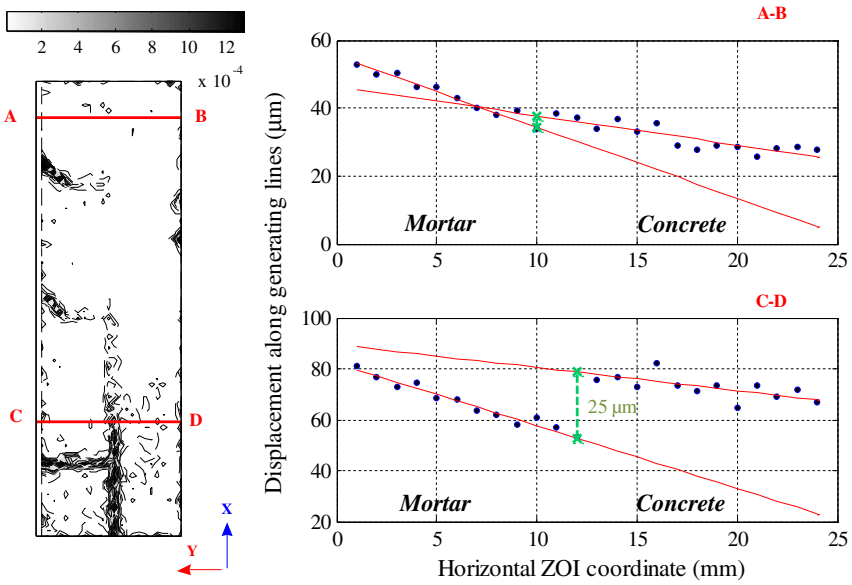

Fig. 11. Determination of the interface crack width by interpolation from the displacement field.

Although there is good agreement between crack widths from DIC observations and widths from microscope observations (see also [28] for more details), the presence of local fluctuations in the displacement fields in both mortar and concrete should be noticed. These fluctuations are due to the correlation process and could result in interpolation errors.

4.2.3. Assessment of interface crack width

The cracking at the interface between mortar and substrate reveals the ability of drying phenomenon to separate the two materials. Thus, the crack width at the interface is an indicator of the damage state of the system. The efficiency of the interpolation method (described previously) to correctly quantify crack widths along the whole interface was verified. For this purpose, displacements were interpolated along two distinct lines crossing the interface. The first one (denoted A–B in Fig. 11) is located in a zone without interface crack whereas the second line (line C–D) crosses such a crack.

In the area without crack (A–B line), the interpolation method procedure gives a gap displacement value lower than the interpolation error. This value does not correspond to a crack width but to the maximum local fluctuation of the calculated displacement. Oppositely, for the line C–D, the so-obtained gap displacement is higher than the interpolation error and it localized at the mortar/substrate interface. A crack width of 25 µm is obtained, which is in good agreement with optical microscopic observation.

Interpolated displacement lines shown in Fig. 11 reveal also that the total strain in the mortar layer is higher than the one in the concrete substrate. This is due to the fact that the drying shrinkage of the mortar layer is (partially) restrained by the concrete substrate: drying shrinkage and mechanical (elastic, creep) strains occur in the mortar layer, while only mechanical strains occur in the concrete substrate.

4.2.4. Reproducibility of the test: comparison of crack widths

Three experiments were conducted on concrete blocks with controlled roughness in order to assess the reproducibility. This

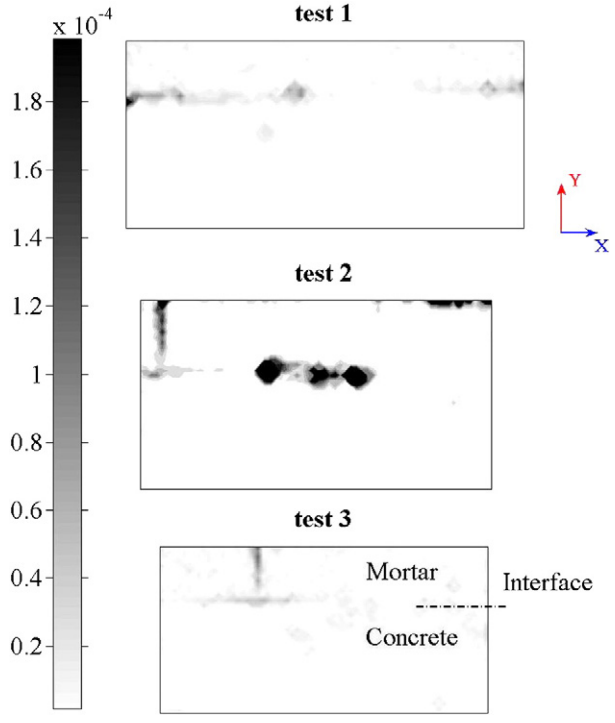

Fig. 12. Comparison of equivalent tensile strength fields (in m/m) in the mortar layer and the concrete substrate after 6 days for the three restrained shrinkage tests (see Section 4.2.4.).

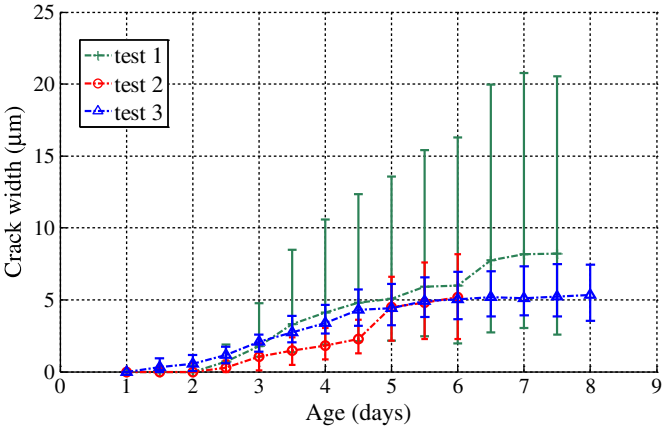

Fig. 13. Time-evolution of the crack width at the interface during the three restrained shrinkage tests (confidence intervals of 75%). Drying begins at the age of 1 day.

study was carried on the zone denoted (2) in Fig. 4 (4×5 cm). The camera recorded the center of the sample in order to avoid edge effects. At the end of the tests, cracks were observed by optical microscopy to determine their location and the order of magnitude of their widths. The crack patterns obtained by means of DIC are given in Fig. 12.

Using the interpolation method (Section 4.2.3), interface crack widths were determined with an assessed resolution of 5 μm. Due to material heterogeneities and random location of defaults, the crack locations and widths observed by optical microscopy were variable from one sample to another. Besides, the interface between the two materials was not locally rectilinear. As a result, crack widths could be overestimated in certain zones. The statistic dispersion along the interface was higher than the measurement resolution. In order to interpret results and avoid artifacts, crack widths were measured at various locations along all interfaces and the interquartile range of this distribution was conserved for comparative study.

For the three tests, the final crack width had approximately the same median value as shown in Fig. 13. Moreover, their global time-evolutions were similar with an initiation of cracking one day after the removal of the formwork and a stabilization of the crack three days after. Note that the dispersion in the test "1" was quite high. However, this method allows us to monitor the evolution and the order of magnitude of cracks of around 10 μm.

5. Conclusion

The crack evolution due to restrained drying shrinkage is hardly measurable but its monitoring is necessary to improve the understanding of mortar/substrate systems behavior. For this purpose, a new experimental method using digital image correlation (DIC) was presented. Based on a post-processing of images obtained by a camera, after painting a random pattern on the studied surface, the device was developed in order to monitor 2D displacement fields.

Firstly, measurements of free drying shrinkage by DIC were compared to those obtained more classically by LVDT sensors. A good concordance between both methods was obtained. Thus, the device makes it possible to monitor continuously small displacement fields during several days.

Secondly, restrained shrinkage tests with concrete substrate were developed to monitor micro-cracks at the drying surface. From the so-measured 2D displacement fields, equivalent tensile strains, such as defined in continuum damage mechanics, can be calculated. Based on a classical criterion (comparison of this equivalent strain with a tensile strain threshold), locations of the cracks can easily be obtained. The proposed method enables a mapping of the cracking surface and a quantification of the total cracked area.

Thirdly, cracking through the thickness of the mortar layer and at the mortar/concrete interface was studied. The proposed method allowed us to assess with a relatively good accuracy and reproducibility crack widths higher than 10 μm.

Based on these results, it can be concluded that DIC method is a promising tool to study coating mortar cracking with representative geometries and in restraint conditions.

Several improvements can be proposed. An alternative to the painting, which could interact with drying, is the use of a video-projector to project a random pattern on the studied surface. Moreover, in order to detect debonding between the mortar layer and the concrete substrate, stereo-correlation (using 2 cameras) can be used so as to measure out of plane displacements of the studied surface. Finally, since cracking due to drying of coating is highly dependent on the boundary conditions (external relative humidity, wind velocity, etc.) and the support (roughness, Young modulus, etc.), a predictive model would be beneficial to analyze cracking phenomenon of coating mortars as observed with DIC.

Acknowledgments

The CEReM consortium, monitored by the CSTB is gratefully acknowledged for its financial support. The second author would like also to thank the National Research Agency (research Project ANR Mefisto) for their partial financial support.

References

[1] O. Omikrine, A. Aït-Mokhtar, A proposed methodology for quantitative investigation of carbonation in polymer-modified mortars, Exp. Tech. 33 (2009) 59–65.
[2] A.H. Al-Gadhib, M.K. Rahman, M.H. Baluch, Prediction of shrinkage and creep stresses in concrete repair systems, ACI Mater. J. 96 (1999) 542–551.
[3] J.C. Amba, J.P. Balayssac, C.H. Detriche, Characterisation of differential shrinkage of bonded mortar overlays subjected to drying, Mater. Struct. 43 (2010) 297–308.
[4] T. Le Bihan, Etude du comportement des chapes autonivelantes en ciment sulfo-alumineux : Outils expérimentaux et de modélisation, PhD Thesis, INSA Lyon, 2010, in french.
[5] O. Laurence, La fissuration due au retrait restreint dans les réparations minces en béton: apport combiné de l'expérimentation et de la modélisation. PhD Thesis, ENPC-Laval University, 2001, in french.
[6] L. Molez, comportement des réparations structurales en beton : couplage des effets hydriques et mécaniques. PhD thesis, ENS Cachan, 2003, in french.
[7] K. Wang, D. Jansen, S.P. Shah, Permeability of cracked concrete, Cem. Concr. Res. 27 (1997) 409–415.
[8] N. Hearn, Effect of shrinkage and load-induced cracking on water permeability of concrete, ACI Mater. J. 96 (1999) 234–241.
[9] P.H. Emmons, A. Vaysburd, Factors affecting the durability of concrete repair: the contractor's viewpoint, Constr. Build. Mater. 8 (1994) 5–16.
[10] D. Cusson, V. Mailvaganarn, Durability of repair materials, Concr. Int. 18 (1996) 34–38.
[11] F. Saucier, F. Claireaux, D. Cusson, M. Pigeon, The challenge of numerical modeling of strains and stresses in concrete repairs, Cem. Concr. Res. 27 (1997) 1261–1270.
[12] A.B. Hossain, J. Weiss, The role of specimen geometry and boundary conditions on stress development and cracking in the restrained ring test, Cem. Concr. Res. 36 (2006) 189–199.
[13] A. Bentur, K. Kovler, Evaluation of early age cracking characteristics in cementitious systems, Mater. Struct. 36 (2003) 183–190.
[14] J. Monge, Fissuration des mortiers en couches minces - Effets de l'hydratation, du séchage et de la carbonatation. PhD Thesis, ENS Cachan, 2007, in french.
[15] M. Briffaut, F. Benboudjema, J.-M. Torrenti, G. Nahas, A thermal active restrained shrinkage ring test to study the early age concrete behavior of massive structures, Cem. Concr. Res. 41 (2011) 56–63.
[16] J. Weiss, W. Yang, S.P. Shah, Shrinkage cracking of restrained concrete slabs, ASCE J. Eng. Mech. 124 (1998) 756–764.
[17] Ph. Turcry, A. Loukili, K. Haidar, G. Pijaudier-Cabot, A. Belarbi, Cracking tendency of self-compacting concrete subjected to restrained shrinkage: experimental study and modeling, J. Mater. Civ. Eng. 18 (2006) 46–54.
[18] A.C.L. Wong, P.A. Childs, R. Berndt, T. Macken, G.D. Peng, N. Gowripalan, Simultaneous measurement of shrinkage and temperature of reactive powder concrete at early-age using fibre Bragg grating sensors, Cem. Concr. Compos. 29 (2007) 1261–1270.
[19] J. Dupont, Comportements de capteurs à fibres optiques, noyés ou fixes en surface d'ouvrage en béton. PhD Thesis, ENPC, 2002, in french.
[20] C.H. Detriche, Analyse experimentale du retrait de couches minces de mortier. Mesure depuis le moulage, Mater. Struct. 11 (1978) 247–259 in french.
[21] J. Bisschop, J.G.M. van Mier, How to study drying shrinkage microcracking in cement-based materials using optical and scanning electron microscopy, Cem. Concr. Res. 32 (2002) 279–287.
[22] H. Colina, P. Acker, Drying cracks: kinematics and scale laws, Mater. Struct. 33 (2000) 101–107.
[23] V. Sicard, R. François, E. Ringot, G. Pons, Influence of creep and shrinkage on cracking in high strength concrete, Cem. Concr. Res. 22 (1992) 159–168.
[24] J. Bisschop, J.G.M. van Mier, Effect of aggregates on drying shrinkage microcracking in cement-based composites, Mater. Struct. 35 (2002) 453–461.
[25] C. Qi, J. Weiss, J. Olek, Characterization of plastic shrinkage cracking in fiber reinforced concrete using image analysis and a modified Weibull function, Mater. Struct. 36 (2003) 386–395.
[26] C.M. Neubauer, H.M. Jennings, E.J. Garboczi, Mapping drying shrinkage deformations in cement-based materials, Cem. Concr. Res. 27 (1997) 1603–1612.
[27] G. Besnard, F. Hild, S. Roux, "Finite-element" displacement fields analysis from digital images: application to Portevin-Le Châtelier bands, Exp. Mech. 46 (2006) 789–804.
[28] F. Lagier, X. Jourdain, C. De Sa, F. Benboudjema, J.B. Colliat, Numerical strategies for prediction of drying cracks in heterogeneous materials: comparison upon experimental results, Eng. Struct. 33 (3) (2011) 920–931 2011.
[29] International Benchmark CONCRACK, synthesis of the results, 2nd Workshop on Control of Cracking in R.C. Structures, ConCrack 2, June 20–22, 2011, Paris, France, 2011, http://cheops.necs.fr/.
[30] M. Küntz, M. Jolin, J. Bastien, F. Perez, F. Hild, Digital image correlation analysis of crack behavior in reinforced concrete beam during a load test, Can. J. Civ. Eng. 33 (2006) 1418–1425.

[31] P. Ienny, A.S. Bretelle, A. Messan, D. Nectoux, Définition et calibration d'une procedure de mesure de champ de deformation sur essais de structures : application à la maturation des mortiers au jeune âge, Photomécanique Symposium, Albi, 2004.
[32] K.C.G. Ong, L.R. Chandra, K. Myint-Lay, Early-age shrinkage strains versus depth of low water–cement ratio mortar prisms, ACI Mater. J. 107 (2010) 213–221.
[33] L. Patural, P. Marchal, A. Govin, P. Grosseau, B. Ruot, O. Devès, Cellulose ethers influence on water retention and consistency in cement-based mortars, Cem. Concr. Res. 41 (2011) 46–55.
[34] Y. Ohama, Polymer-based admixtures, Cem. Concr. Compos. 20 (1998) 189–212.
[35] P.M.D. Santos, E.N.B.S. Julio, V.D. Silva, Correlation between concrete-to-concrete bond strength and the roughness of the substrate surface, Constr. Build. Mater. 21 (2007) 1688–1695.
[36] A. Garbacz, L. Courard, K. Kostana, Characterization of concrete surface roughness and its relation to adhesion in repair sytems, Mater. Charact. 56 (2006) 281–289.
[37] C. De Sa, F. Benboudjema, M. Thiery, J. Sicard, Analysis of microcracking induced by differential drying shrinkage, Cem. Concr. Compos. 30 (2008) 947–956.
[38] F. Hild, B. Raka, M. Baudequin, S. Roux, F. Cantelaube, Multi-scale displacement field measurements of compressed mineral wool samples by digital image correlation, Appl. Opt. 32 (2002) 6815–6828.
[39] F. Hild, S. Roux, Full-field Measurement and Identification in Solid Mechanics, KMM-NoE Network of Excellence, Warsaw, 2007.
[40] F. Hild, S. Roux, CORRELIQ4: A Software for "Finite-element" Displacement Field Measurements by Digital Image Correlation, April 2008, Internal report no. 269, LMT, ENS CACHAN, 2008, available at, http://www.lmt.ens-cachan.fr/PDFs/HILD.2008.7.pdf.
[41] J. Mazars, A description of micro and macroscale damage of concrete structures, Eng. Fract. Mech. 25 (1986) 729–737.
[42] Z.P. Bažant, Y. Xi, Drying creep of concrete: constitutive model and new experiments separating its mechanisms, Mater. Struct. 27 (1994) 3–14.
[43] A. Aït-Mokhtar, O. Amiri, S. Sammartino, Analytic modelling and experimental study of the porosity and the permeability of porous media, appliation to cement mortars and granitic rocks, Mag. Concr. Res. 51 (1999) 391–396.